Quaternary Geochronology 5 (2010) 503–511

Contents lists available at ScienceDirect

Quaternary Geochronology

journal homepage: www.elsevier.com/locate/quageo

Research Paper

Eruption ages of Las Tres Vírgenes volcano (Baja California): A tale of two helium isotopes

Axel K. Schmitt [a,*], Daniel F. Stockli [b], Samuel Niedermann [c], Oscar M. Lovera [a], Brian P. Hausback [d]

[a] Department of Earth and Space Sciences, University of California Los Angeles, 595 Charles Young Drive E, Los Angeles, CA 90095, USA
[b] Department of Geology, University of Kansas, 120 Lindley Hall, 1475 Jayhawk Boulevard, Lawrence, KS 66045-7613, USA
[c] Helmholtz-Zentrum Potsdam, Deutsches GeoForschungsZentrum, Telegrafenberg, D-14473 Potsdam, Germany
[d] Geology Department, California State University, Sacramento, CA 95819-6043, USA

ARTICLE INFO

Article history:
Received 4 September 2009
Received in revised form
11 February 2010
Accepted 15 February 2010
Available online 21 February 2010

Keywords:
Uranium series
Zircon
Cosmogenic nuclides
Tephrochronology
^{14}C dating

ABSTRACT

La Virgen tephra is the product of the youngest and most voluminous explosive eruption of Las Tres Vírgenes volcano (Baja California). Combined U–Th and (U–Th)/He zircon dating allows accurate correction for uranium-series disequilibrium, and yields an eruption age for La Virgen tephra of $30.7^{+1.8}_{-1.4}$ ka (2σ). No difference in eruption ages was found between samples from proximal and distal La Virgen tephra. A previously undated tephra south of Las Tres Vírgenes volcano yielded U–Th and (U–Th)/He zircon ages overlapping those of La Virgen tephra, which suggests that both units are identical. ^{3}He surface exposure ages (T_3) of overlying mafic lavas are 25.5 ± 4.4 and 22.0 ± 2.5 ka, and agree within uncertainties with ^{21}Ne exposure ages (T_{21}). T_3 and T_{21} ages for dome lava south of La Virgen are slightly older ($T_3 = 42.5 \pm 3.8$ ka). (U–Th)/He and surface exposure ages are stratigraphically consistent, whereas a published Holocene ^{14}C charcoal age from the distal site could not be confirmed. Instead, abundant zircon crystals with (U–Th)/He ages between ~1 and 22 Ma are interpreted as undegassed detrital grains, suggesting reworking of pumice at the distal location. The results presented here underscore the potential of combined U–Th and (U–Th)/He zircon dating for Quaternary tephrochronology.

1. Introduction

(U–Th)/He zircon dating has demonstrably high potential for Quaternary volcanic chronostratigraphy, but corrections for uranium decay series (U-series) disequilibrium remain a significant source of uncertainty, especially for protracted crystallization and variable pre-eruptive crystal residence times that are common in many volcanic systems (e.g., Farley et al., 2002). Previously published Late Pleistocene (U–Th)/He zircon ages for La Virgen tephra, which erupted from Las Tres Vírgenes volcano (Baja California), met with controversy because conflicting age constraints exist from historical records and various radiometric dating techniques (Schmitt et al., 2006, 2007; Capra et al., 2007). For example, Ives (1962) interpreted that Las Tres Vírgenes was historically active based on a map drawn by the Jesuit missionary Ferdinand Konščac (Ferdinando Consag) in his narrative of travel along the coast of Baja California during 1746 CE. By contrast, Capra et al. (1998) report an uncalibrated ^{14}C age of ~6500 a BP for charcoal from a distal La Virgen tephra deposit. This age, however, was found to be stratigraphically inconsistent with concordant (U–Th)/He zircon ages for La Virgen tephra (36 ± 6 ka at 2σ uncertainty; Schmitt et al., 2006) and the ^{3}He exposure age for overlying basalt lava (26 ± 8 ka; Hausback and Abrams, 1996).

Because the sample dated by the (U–Th)/He zircon method in Schmitt et al. (2006) was from a different locality than the ^{14}C-dated charcoal sample of Capra et al. (1998), ambiguity remained whether the ages refer to the same eruption. Earlier (U–Th)/He zircon ages were corrected for disequilibrium by assuming a uniform crystallization age estimated from the peak in the U–Th age distribution for a composite population of La Virgen zircon (Schmitt et al., 2006). This was a simplifying assumption due to lack of better age constraints for zircon aliquots that lacked ion microprobe U–Th crystallization ages.

We subsequently explored combined (U–Th)/He and U–Th dating of single zircon crystals to reduce potential bias for zircon populations with heterogeneous crystallization ages. Here, we report ages for La Virgen zircon determined by this method, including samples from the Capra et al. (1998) charcoal location. We also introduce a refined computational tool for (U–Th)/He disequilibrium corrections that calculates eruption ages and

* Corresponding author. Tel.: +1 310 206 5760; fax: +1 310 825 2779.
E-mail address: axel@oro.ess.ucla.edu (A.K. Schmitt).

1871-1014/$ – see front matter © 2010 Elsevier B.V. All rights reserved.
doi:10.1016/j.quageo.2010.02.004

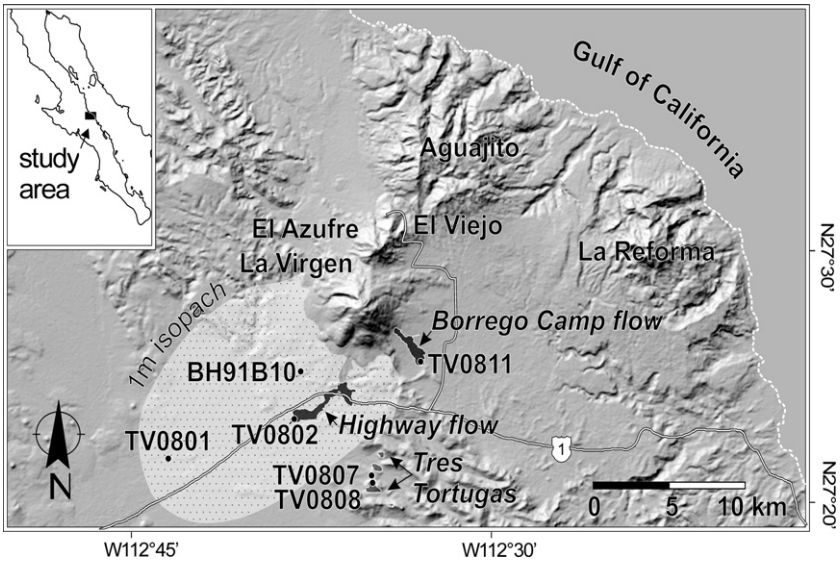

Fig. 1. Sketch map of the Volcán Las Tres Vírgenes complex (comprising the edifices of La Virgen, El Azufre and El Viejo). Extent of sampled lava flows and La Virgen tephra is shown along with sampling locations. Map based on Aster Global digital elevation model at 30 m resolution and own field observations.

uncertainties for individual analyses, and goodness-of-fit parameters in order to assess age concordancy in crystal populations. Eruption ages for La Virgen tephra sampled at the same site as the previously published ^{14}C charcoal sample are compared to new cosmogenic nuclide exposure ages of lava flows to verify stratigraphic consistency.

2. Geological setting

The complex of Volcán Las Tres Vírgenes (Fig. 1) is located within the Gulf of California rift zone, and is part of a volcanic ridge that extends from the eastern coast of Baja California towards active seafloor spreading centers in the Guaymas basin (Fabriol et al., 1999). Volcanism progressed in a counter-clockwise sense from La Reforma caldera to the E (~1.6–1.4 Ma), the Aguajito centers to the NE (~1.2–0.5 Ma), and the central vent edifices of El Viejo and El Azufre to the N (Demant, 1981; Garduno-Monroy et al., 1993; Schmitt et al., 2006). The morphologically dominating and most recent volcanic center is the ~15 km^3 La Virgen edifice (Sawlan, 1986; Capra et al., 1998), which comprises early cone-building effusive deposits, overlain by pyroclastic deposits from a later phase of explosive activity. None of these early deposits are radiometrically dated. Las Tres Vírgenes activity culminated in the deposition of the >1.14 km^3 La Virgen tephra which is dispersed in a ~500 km^2 area to the SW of the volcano (Sawlan, 1986; Hausback and Abrams, 1996; Capra et al., 1998). Because of its volume and the volcanic hazard potential of Plinian eruption columns, La Virgen tephra is a key stratigraphic unit whose eruption age has been targeted by several geochronologic studies, yielding conflicting results between ~6500 a BP (Capra et al., 1998) and 36 ± 6 ka (Schmitt et al., 2006).

Younger mafic (basalt to basaltic-andesite) lava flows overlying La Virgen tephra erupted from the flanks of the volcano in two extensive lobes that are 3.4 km and 2.7 km in length, respectively (Fig. 1). We informally name the southern flow Highway Basalt and the southeastern flow Borrego Camp Basaltic-Andesite. A single ^{3}He exposure age for the Highway Basalt flow of 26 ± 8 ka (Hausback and Abrams, 1996) exists, but no age constraints are available for the Borrego Camp flow. Three morphologically young mafic domes occur south of Las Tres Vírgenes, and are termed here Las Tres Tortugas. Geothermal surface manifestations underlain by a geothermal reservoir are located at the NE base of the volcano. The reservoir is currently exploited for geothermal electricity generation for the nearby port town of Santa Rosalía (Verma et al., 2006).

3. Materials and methods

3.1. Sampling and locations

In January 2008, we sampled La Virgen tephra at the same location from which Capra et al. (1998) recovered a single fragment of charcoal for ^{14}C dating. The location is on an elevated terrace near the southern edge of a 1 km broad ephemeral stream channel, ~18 km to the southwest of the eruptive vent. We excavated a 1.2 m deep dig to establish the stratigraphy and to sample pumice (Fig. 2). The base of the section is formed by stream-bed cobbles (layer 1). It is overlain by a 60 cm deposit of poorly sorted subangular to rounded pumice with a maximum diameter of 12 mm (layer 2) and minor sand. Between 60 cm depth and the surface, the deposit consists of sand mixed with rounded pumice (max. diameter 30 mm), and is penetrated by abundant plant roots (layer 3). TV0801 is a composite pumice sample from layer 2, collected within 15 cm of the contact to the underlying cobble bed (layer 1).

At another location between the middle and the southern Tres Tortugas dome, we collected a composite pumice sample (TV0807) from a well-sorted deposit of light-colored lapilli (maximum diameter 15 mm). The base of this deposit with a thickness of ~40 cm is not exposed, but it is overlain by a 10–15 m section of dark scoriaceous air-fall deposits exposed in a steeply flanked arroyo.

For sampling original aa lava flow surfaces, we targeted large blocks or spires (several m^2 in cross section) that lack any indication of post-emplacement movement. The top 5 cm of scoriaceous flow surfaces were removed from the center of these blocks using hammer and chisel. Sampled surfaces were from locations that have unobstructed views of the sky, and lack vegetation, soil or ash cover. Despite care of selecting sample locations based on the criteria outlined above, potentially unrecognized erosion of the aa lava flow surfaces would result in cosmogenic dates being

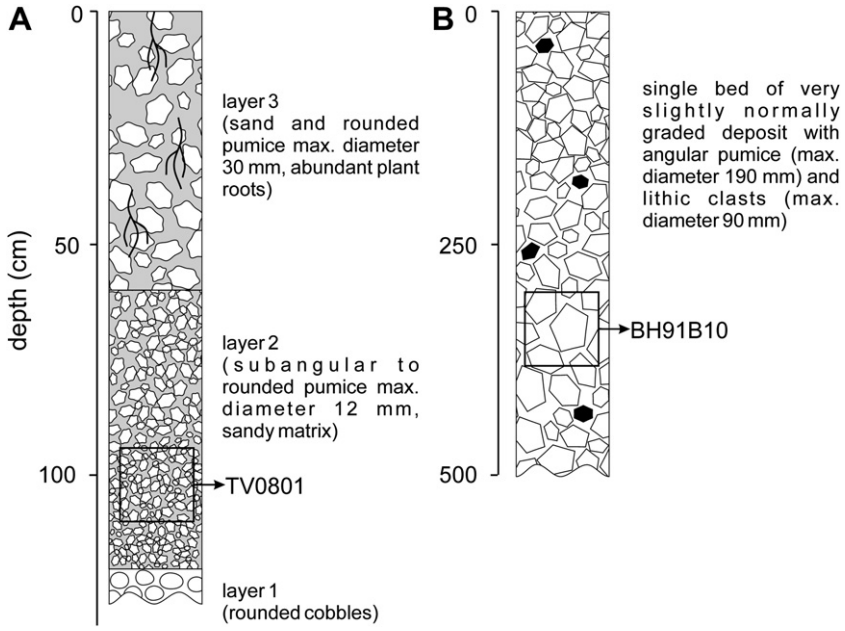

Fig. 2. Stratigraphic columns for sample locations (A) TV0801 (equivalent to TV9564 in Capra et al., 1998, 2007) and (B) BH91B10 (Schmitt et al., 2006). Boxes indicate horizons from which composite pumice samples for (U–Th)/He zircon dating were collected. The charcoal dated by Capra et al. (1998) was recovered near the base of layer 2.

minimum ages. The dated samples (Fig. 1) are from Highway Basalt flow (TV0802), Borrego Camp Basaltic-Andesite flow (TV0811), and the southern Tres Tortugas dome (TV0808).

3.2. Sample preparation

Approximately 1 kg of composite pumice clasts were sieved to >6 mm and ultrasonically washed, which caused separation between pumice that floated and dense rocks such as lithic clasts and sand that sank. We note that this procedure only incompletely removed fine-grained sediment adherent to the pumice surfaces. Pumice was subsequently dried at room temperature, crushed, and sieved to <250 μm. One aliquot of the <250 μm fraction was digested in HF, another immersed in heavy liquids (tetrabromethane, diiodomethane) to concentrate zircon. Zircon crystals typically ~100–300 μm long and ~50–100 μm wide were hand-picked from both concentrates under a binocular microscope, and pressed into indium (In) metal with crystal surfaces flush on the surface for ion microprobe analysis without any surface preparation besides ultrasonic cleaning, and coating with a conductive layer of 20–30 nm of Au. Subsequent to ion microprobe analysis, grains were extracted from the In with a steel needle, photographed, and packed into platinum (Pt) tubes for He degassing (see below).

Surface exposure dating was performed on olivine and pyroxene separated from 3 to 5 kg rock sample from the top 5 cm of the hand samples. Olivine and pyroxene were concentrated after crushing and sieving from the 250 to 425 and 425 to 850 μm size fractions through magnetic and heavy liquid separation, followed by hand-picking under a binocular microscope. Petrographic thin-sections show that crushing did not significantly reduce crystal sizes. Aliquots of the separates were analyzed for major element compositions by electron microprobe, and found to be >97% free from groundmass. Moreover, additional aliquots as well as bulk groundmass samples were ground to <2 μm powder, digested by acid dissolution, and analyzed by inductively coupled plasma mass spectrometry (ICP-MS) to determine U and Th abundances for radiogenic ^{4}He corrections.

3.3. U–Th ion microprobe analysis

Ion microprobe protocols for U–Th analysis using the CAMECA ims 1270 at UCLA followed those described in Schmitt et al. (2006). In addition to ~25 min spot analyses on unpolished rims (depth resolution 5 μm), grain BH91B10 z20 was selected for continuous depth profiling from rim to ~30 μm depth. Accuracies of the relative sensitivity calibration for U/Th and background corrections were monitored by replicate analysis of equilibrium zircon standard AS3 mounted next to the unknowns (1099.1 Ma; Paces and Miller, 1993). The average for AS3 analyzed interspersed with the unknowns yielded a unity secular equilibrium ratio for (^{230}Th)/(^{238}U) = 0.998 ± 0.010 (activities denoted in parentheses; MSWD = 2.2; n = 8). Uranium concentrations were estimated from $UO^{+}/Zr_2O_4^{+}$ intensity ratios relative to zircon standard 91500 (81.2 ppm U; Wiedenbeck et al., 2004). Crystallization ages were calculated as two-point zircon – melt isochrons using La Virgen tephra whole-rock compositions in Schmitt et al. (2006).

3.4. (U–Th)/He analysis

(U–Th)/He age determinations were carried out at the University of Kansas using laboratory procedures described in Biswas et al. (2007). Zircon crystals were wrapped in Pt foil, heated for 10 min at 1290 °C and reheated until >99% of the He was extracted from the crystal. All ages were calculated using standard α-ejection corrections using morphometric analyses (Farley et al., 1996). After laser heating, zircon crystals were unwrapped from the Pt foil and dissolved using double-step HF–HNO_3 and HCl pressure-vessel digestion procedures (Krogh, 1973). U, Th, and Sm concentrations were determined by isotope dilution ICP-MS analysis. The laboratory routinely analyzes zircon standards with independently determined ages, and we report averages for Fish Canyon tuff zircon of 27.8 ± 0.8 Ma (RSD% = 7.5%, n = 285) and Durango zircon of 30.2 ± 1.1 Ma (RSD% = 6.8; n = 76). From the reproducibility of replicate analyses of these laboratory standard samples we estimate analytical uncertainties of 8% (1σ) for individual zircon (U–Th)/He ages.

3.5. Surface exposure dating

Approximately 0.65–1.50 g samples of the olivine/pyroxene separates of TV0802, TV0808, and TV0811 were weighed, wrapped in Al foil, and loaded into the sample carrousel of the ultrahigh vacuum furnace at the GFZ Potsdam noble gas lab. Noble gases were extracted by stepwise heating at 600, 900, and 1750 °C. Active gases were removed in a dry ice trap, two titanium sponge or foil getters, and two SAES (Zr–Al) getters. The noble gases were then trapped at 11 K on activated charcoal in a cryogenic adsorber and sequentially released for separate He, Ne, and Ar–Kr–Xe analysis in a VG5400 noble gas mass spectrometer. Corrections for isobaric interferences of $^{40}Ar^{++}$ at $m/e = 20$ and $^{12}C^{16}O^{++}$ at $m/e = 22$ were applied according to Niedermann et al. (1997); a correction for $H_2^{18}O^+$ at $m/e = 20$ was not necessary due to the mass resolution of $\geq$600 of the VG5400. Analytical blanks were 10^{-11}–10^{-10} cm^3 STP for ^{4}He and 0.6–2.2 $\times 10^{-12}$ cm^3 STP for ^{20}Ne depending on extraction temperature, with atmospheric isotopic compositions. This corresponds to 400–4000 atoms ^{3}He and 50,000–170,000 atoms ^{21}Ne.

Before being loaded to the extraction furnace, the TV0802 and TV0811 samples had been crushed in vacuo in order to determine the isotopic composition of He and Ne trapped in fluid inclusions. From TV0808 enough material was available to use a separate aliquot for the crushing extraction. In our manually operated crusher, samples are simply squeezed between two hard metal jaws, which minimizes the possibility for any loss of cosmogenic He. Crusher blanks were $\sim 4 \times 10^{-12}$ cm^3 STP and 0.5×10^{-12} cm^3 STP for ^{4}He and ^{20}Ne, respectively.

3.6. Correction procedures for combined U–Th and (U–Th)/He dating

Zircon crystallization results in significant disequilibrium in U-series decay chains (e.g., Farley et al., 2002). Deficits in intermediate daughter isotopes (mainly ^{230}Th with a half-life of ~75.7 ka) at the time of eruption will lead to retardation in ^{4}He accumulation compared to a crystal that is in secular equilibrium, and consequently an underestimation of the eruption age. Other longer-lived daughter isotopes that can be fractionated from parental U isotopes are ^{231}Pa (half-life ~32.8 ka) and ^{226}Ra (half-life ~1.6 ka). Disequilibria in ^{231}Pa and ^{226}Ra, however, have only minor and compensatory effects on (U–Th)/He zircon ages, so that they can be reasonably neglected except for zircon with very young crystallization ages (Farley et al., 2002).

If the magma was in secular equilibrium, as is the case of La Virgen tephra (Schmitt et al., 2006), the deficit in ^{230}Th at the time of zircon crystallization can be calculated from the D_{230} parameter (Farley et al., 2002):

$$D_{230} = (\mathrm{Th/U})_{\mathrm{zircon}}/(\mathrm{Th/U})_{\mathrm{magma}} \quad (1)$$

whereby $(\mathrm{Th/U})_{\mathrm{magma}}$ is approximated from whole-rock or matrix glass compositions. The amount of initial U-series disequilibrium in zircon described by D_{230}, however, will diminish due to radioactive ingrowth of ^{230}Th if sufficient time elapses between zircon crystallization and eruption. Crystal residence at elevated temperature or reheating at the time of eruption prevents ^{4}He accumulation in zircon. Thus, constraining the effective D_{230} at the time of eruption ($^{\mathrm{eruption}}D_{230}$) is critical for accurate disequilibrium correction of young (U–Th)/He ages.

In order to determine $^{\mathrm{eruption}}D_{230}$ and to correct (U–Th)/He ages, we developed a Monte Carlo computational routine ("MCHeCalc") that calculates probability density functions for disequilibrium-corrected (U–Th)/He ages based on the following input variables: (1) uncorrected (U–Th)/He ages, (2) U–Th crystallization ages, and (3) D_{230} (at the time of crystallization). In the computation, a (U–Th)/He age is first randomly picked from the Gaussian distribution represented by the equilibrium age and its uncertainty (standard error σ). Then, an associated crystallization age is randomly picked from the measured crystallization age Gaussian distribution as described above. In a third step, each randomly picked (U–Th)/He age is corrected for disequilibrium by calculating $^{\mathrm{eruption}}D_{230}$ using the differential equations for n-nuclide decay series (Bateman, 1910) and the corresponding random pick from the crystallization age distribution.

Monte Carlo calculations of the eruption age probability density functions comprise 100,000 or 1,000,000 trials per individual analysis. The software is designed to disregard and repeat trials that violate the constraint that eruption must post-date crystallization. The resulting eruption age distributions are usually pseudo-Gaussian with slightly asymmetric standard deviations. A "concordant" eruption age probability density function is calculated from the intersection of all individual eruption age distributions. This "concordant" age distribution is also pseudo-Gaussian and can be represented by its peak age and its asymmetric associated uncertainties. Finally, the program estimates a goodness-of-fit parameter Q using the regularized gamma function (Press et al., 2002):

$$Q = \mathrm{gammq}\left[(n-1)/2, \chi^2/2\right] \quad (2)$$

where χ^2 is the "chi-square" between the "concordant" eruption age and the individual zircon eruption ages, and n is the number of measurements. A model fit is considered acceptable if $Q \geq 0.001$ (Press et al., 2002).

For testing of our computational routine, we modeled published Rangitawa tephra zircon data of known eruption age (330 ka; Farley et al., 2002) that show crystal residence times between 0 and >380 ka (i.e., secular equilibrium). By reproducing the independently determined 330 ka eruption age of Rangitawa tephra (Farley et al., 2002) to within <2%, we confirmed the reliability of our computational routine (MCHeCalc age: 326 ± 6 ka; $n = 15$; goodness-of-fit of 0.99). The MCHeCalc program (MCHeCalc.exe) and the Rangitawa test file (Farley.in) can be obtained at request from the authors.

4. Results

4.1. La Virgen tephra zircon

U–Th zircon rim ages for La Virgen tephra sample TV0801 (Table 1) range between ~34 ka and >380 ka (secular equilibrium). The crystallization age distribution for zircon rim ages of TV0801 extends to younger ages relative to BH91B10 zircon interiors (Schmitt et al., 2006), but rim and interior ages overlap (Fig. 3). Continuous depth profiling of grain BH91B10 z20 (Fig. 4) yielded a rim age of 59^{+22}_{-20} ka (2σ; MSWD = 0.63; 0–7.5 μm), whereas the core age averages 157^{+36}_{-34} ka (MSWD = 1.1; 7.5–22.5 μm). Conventional ion microprobe spot analyses of the same crystal at a lateral resolution of 20–25 μm yielded ages of 129^{+48}_{-40} ka ("rim") and 200^{+86}_{-62} ka (interior; Fig. 3). The interior spot age overlaps within uncertainty with the core depth profiling age. The rim spot age, however, is older than the unpolished rim analyzed in depth profiling. This is likely due to beam overlap onto interior age domains during spot analysis.

Approximately one third (five out of 13) of the TV0801 zircon rim analyses yield secular equilibrium ages (Table 1). Secular equilibrium grains are thus nearly twice as abundant in TV0801 compared to previously dated sample BH91B10 with three grains

Table 1
Combined U–Th and (U–Th)/He zircon dating results, error limits are 2σ.

Zircon	(^{238}U)/(^{232}Th)		(^{230}Th)/(^{232}Th)		U–Th age (ka)			U (ppm)	Th (ppm)	D_{230}	He (nmol/g)	Ft	Equilibrium (U–Th)/He age (ka)		Disequilibrium (U–Th)/He age (ka)			Remarks
		±		±		+	−							±		+	−	
TV0801eruption age: 29.1 +2.2/−2.0 ka (Q = 0.0012)																		
z1	6.94	1.14	8.18	1.55	∞	∞	∞	279	130	n.a.	n.a.	n.a.	n.a.	n.a.	n.a.	n.a.	n.a.	
z2	8.63	0.19	4.48	1.22	65	38	28	95.1	61.4	0.23	0.0109	0.77	24.2	3.9	34.6	8.5	6.6	a
z3	7.77	0.09	2.88	0.67	34	16	14	95.0	87.5	0.32	0.0112	0.80	22.5	3.6	33.7	5.6	5.6	a
z4	6.39	0.20	2.98	0.45	48	16	14	127	128	0.35	0.0116	0.71	19.2	3.1	26.6	4.6	4.7	a
z5	8.28	0.14	8.40	1.11	∞	∞	∞	72.8	31.7	0.15	7.03	0.77	21,100	3,400	*	*	*	b
z11	5.34	0.12	5.11	0.32	325	∞	103	329	240	0.25	33.3	0.72	22,400	3,600	*	*	*	b
z12	9.38	0.28	4.74	0.83	64	22	18	162	55.9	n.a.	n.a.	n.a.	n.a.	n.a.	n.a.	n.a.	n.a.	
z13	6.65	0.07	7.29	0.98	∞	∞	∞	80.8	41.2	0.18	0.0156	0.87	37.0	5.9	*	*	*	c
z14	6.48	0.08	6.68	0.89	∞	∞	∞	122	60	0.17	0.627	0.78	1,100	180	*	*	*	b
z15	6.56	0.07	6.47	0.94	466	∞	282	184.5	91.2	n.a.	n.a.	n.a.	n.a.	n.a.	n.a.	n.a.	n.a.	
z16	7.19	0.09	4.02	0.78	72	31	24	123	114	0.32	0.0111	0.77	18.0	2.9	23.4	4.6	4.0	a
z17	6.29	0.08	6.64	0.77	∞	∞	∞	53.9	26.5	0.17	0.263	0.85	950	160	*	*	*	b
z18	7.30	0.35	3.01	0.78	41	22	18	90.1	48.1	0.19	0.0126	0.82	28.1	4.5	46.7	8.2	7.4	c
TV0807 eruption age: 30.6 + 2.8/−2.4 ka (Q = 0.0093)																		
z1	8.16	0.24	6.41	0.95	153	90	49	145	88.9	0.21	0.0209	0.82	28.5	4.6	32.8	7.2	5.4	a
z2	8.83	0.36	3.90	0.70	49	17	15	147	74.9	0.18	0.0278	0.80	39.4	6.3	63.6	14.4	8.8	c
z3	9.93	0.19	7.08	1.07	124	52	35	79.4	42.9	0.19	0.00816	0.79	21.3	3.4	25.9	5.7	4.2	a
z4	3.58	0.11	2.40	0.17	82	18	15	140	98.9	0.25	0.0158	0.74	24.2	3.9	32.4	5.9	5.4	a
z6	7.25	0.14	3.69	0.91	60	32	25	172	94.4	0.19	0.0154	0.86	17.2	2.7	26.1	5.6	6.0	a
z7	4.77	0.08	3.23	0.38	96	32	25	451	306	n.a.	n.a.	n.a.	n.a.	n.a.	n.a.	n.a.	n.a.	
z8	5.48	0.09	3.50	0.45	88	29	23	289	171	n.a.	n.a.	n.a.	n.a.	n.a.	n.a.	n.a.	n.a.	
BH91B10 z2 depth profiling results																		
0–3.8	2.26	0.08	3.05	0.93	49	35	26	139	69.1									
3.8–7.5	2.26	0.03	3.53	0.78	66	34	26	161	80.5									
7.5–11.3	1.89	0.05	4.83	0.70	218	∞	89	191	114									
11.3–15.0	1.72	0.02	3.64	0.59	119	68	42	252	165									
15.0–18.8	1.64	0.02	3.54	0.56	124	74	44	291	200									
18.8–22.5	1.61	0.02	4.15	0.62	221	∞	95	306	214									
22.5–26.3	1.77	0.01	4.29	0.89	177	∞	83	272	173									
26.3–30	1.89	0.02	4.42	0.90	159	254	70	240	143									
"Rim"	1.27	0.03	2.86	0.29	129	55	37	318	282									
"Interior"	1.42	0.03	3.59	0.28	200	116	55	332	264									

Sample locations (WGS-84): TV0801 = N27°22′05″, W112°43′50″; TV0807 = N27°21′51″, W112°35′02″; BH91B10 = N27°25′42″, W112°37′43″.
∞ secular equilibrium; n.a. = not analyzed; * = no correction applied (secular equilibrium).
U–Th age from slope through zircon and whole-rock (Schmitt et al., 2006) composition.
Parentheses denote activities; $D_{230} = [^{232}Th/^{238}U]_{zircon}/[^{232}Th/^{238}U]_{whole\text{-}rock}$; Ft = alpha particle ejection correction parameter.
Decay constants used: λ_{230}: 9.1577×10^{-6} a^{-1}; λ_{232}: 4.9475×10^{-11} a^{-1}; λ_{238}: 1.55125×10^{-10} a^{-1}; $\lambda_{226} = 4.332 \times 10^{-4}$ a^{-1}.
Zircon U-series analyses by ion microprobe.
Zircon(U–Th)/He analysis by inductively coupled mass spectrometry (U, Th), and quadrupole mass spectrometry (He).
a = Disequilibrium-corrected age used for weighted average.
b = Excluded from weighted average (detrital).
c = Equilibrium age used for weighted average.

out of 14 in secular equilibrium (Schmitt et al., 2006). Even more striking is the difference between (U–Th)/He ages for secular equilibrium zircon in both samples: four TV0801 secular equilibrium zircon crystals yielded comparatively old (U–Th)/He ages between ~1 and 22 Ma (Table 1), much older than the remaining ages between ~18 and ~37 ka (prior to correction for disequilibrium; Table 1). This is in contrast to previously dated zircon crystals from BH91B10 that show entirely Late Pleistocene (36 ± 6 ka) (U–Th)/He ages, despite the fact that some of these crystals have Mid Cenozoic to Early Mesozoic crystallization ages. Secular equilibrium crystals in proximal sample BH91B10 thus became completely degassed at the time of eruption, whereas those in distal sample TV0801 preserved pre-eruptive (U–Th)/He ages. The exception is TV0801 z13 with a secular equilibrium U–Th rim age and a Late Pleistocene (U–Th)/He age.

Monte Carlo models for TV0801 zircon (disequilibrium-uncorrected average: 22.3 ± 5.3 ka) were run using the overall average U–Th age (146 ± 110 ka) or individual U–Th rim ages as estimates for the crystallization age of the entire grain (Fig. 5). In both cases, the disequilibrium-corrected age of grain TV0801 z18 is an outlier to older ages, resulting in very low probabilities for the model ($Q = 1.4 \times 10^{-7}$ and 2.8×10^{-7}, respectively). Because zircon age zonation is demonstrably present in La Virgen zircon (Fig. 4), the ~41 ka rim age of TV0801 z18 is regarded as a minimum for the bulk crystallization age. When re-calculated assuming equilibrium, grain z18 falls in line with the rest of the population, and Q increases significantly ($29.1^{+2.2}_{-2.0}$ ka; $Q = 0.0012$; Fig. 5C). Individually disequilibrium-corrected ages (Table 1) thus yield the best results, with the caveat that potential age zonation could lead to overcorrected (=too old) eruption ages.

For sample TV0807, the uncorrected average (U–Th)/He zircon age is 22.5 ± 8.4 ka. Disequilibrium correction using individual rim U–Th ages or the average U–Th age increases the eruption age estimate, but results in low probabilities of fit because of outlier grain TV0807 z2 ($Q = 7 \times 10^{-13}$ and 3×10^{-6}, respectively). Assuming equilibrium for the bulk of grain TV0807 z2, a much better overall fit is obtained for the individually corrected ages (Fig. 5G). The average age of $30.6^{+2.8}_{-2.4}$ ka ($Q = 0.009$) is indistinguishable from that of the other locations.

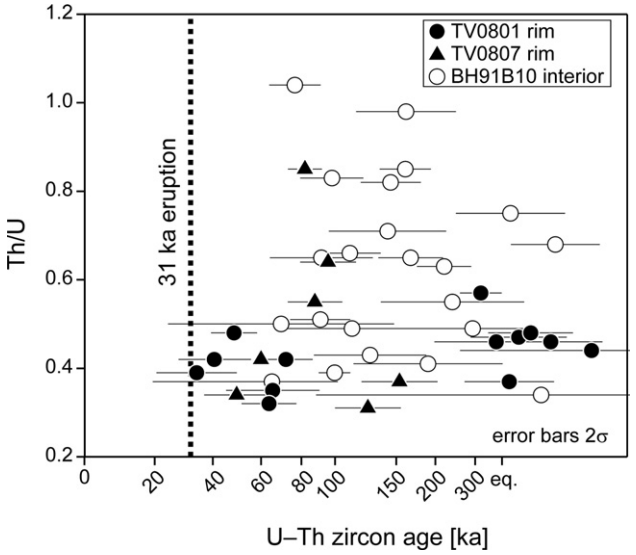

Fig. 3. U–Th zircon crystallization ages and Th/U in zircon for TV0801 (distal La Virgen) and TV0807 (tephra near Tres Tortugas) in comparison to published data BH91B10 (Schmitt et al., 2006). Eruption age is indicated based on disequilibrium-corrected (U–Th)/He zircon ages.

4.2. Mafic lavas

The results of He and Ne analyses of olivine/pyroxene separates from surface mafic lavas are presented in Table 2. According to the crushing extractions of TV0802 and TV0808, the magmatic $^3He/^4He$ ratio in Tres Vírgenes olivine and pyroxene is $(10.15 \pm 0.90) \times 10^{-6}$ (weighted mean), or 7.30 ± 0.65 R_A, where R_A is the atmospheric $^3He/^4He$ ratio of 1.39×10^{-6}. We do not consider the result from TV0811, which released an order of magnitude less He than the other two samples during crushing. The cosmogenic ^3He concentrations (^3He_c) shown in Table 3 have been calculated from the stepwise heating data according to

$$^3He_c = \left[(^3He/^4He)_{measured} - (^3He/^4He)_{magmatic}\right] \times {}^4He_{measured}/R \quad (3)$$

and summing up the three heating steps. R is a correction factor proposed by Blard and Farley (2008), who have pointed out that ^3He exposure ages may be underestimated when the possible presence of radiogenic ^4He in the olivine or pyroxene minerals is not taken into account. ^4He is being produced since eruption of the lava by U and Th decay, either in the mafic lava matrix and injected into the phenocrysts or within the phenocrysts. To assess the possible influence of radiogenic ^4He, we have determined U and Th concentrations in both the matrix and the phenocrysts by ICP mass spectrometry at the GFZ Potsdam. The results (Table 4) indicate a ^4He production of $0.02–0.11 \times 10^{-8}$ cm^3 STP/g in the phenocrysts during their exposure ages, assuming a stopping distance of α particles of 20 μm and an average crystal diameter of 350 μm (using equation (2) of Blard and Farley, 2008). This corresponds to 1.8–5.1% corrections to the cosmogenic ^3He concentrations, or R factors of 0.949–0.982 (Table 4). As the size of the phenocrysts varies and their shape is not ideally spherical, we assign a conservative 50% uncertainty (i.e., $(1 - R)/2$) to these corrections.

For Ne, the crushing extractions as well as the 600 °C and 900 °C data showed essentially atmospheric isotopic composition. In a three-isotope plot (not shown), the 1750 °C data lie on the mixing line of air and cosmogenic Ne (Schäfer et al., 1999) within uncertainties. Therefore, cosmogenic ^{21}Ne (Table 3) was obtained as the excess over atmospheric abundances and is dominantly determined by the 1750 °C step.

To calculate surface exposure ages from the cosmogenic ^3He and ^{21}Ne concentrations, the production rates at the sampling location for the respective mineral chemistry have to be known. While the ^3He production rate depends only slightly on chemical composition (e.g. Masarik, 2002), the ^{21}Ne production rate varies substantially, in particular with Mg content. In the past, production rates of ^3He and ^{21}Ne as obtained by experimental determinations (e.g. Cerling and Craig, 1994; Licciardi et al., 1999) or physically-based model calculations (e.g. Masarik, 2002; Kober et al., 2005) have yielded inconsistent ^3He and ^{21}Ne exposure ages (Niedermann et al., 2007; Fenton et al., 2009). Here we use the method of Fenton et al. (2009) to calculate sea level/high latitude production rates (Table 3) based on the major element composition of each sample as determined by microprobe analysis (Table 5). These authors adjusted the model data of Masarik (2002) to the experimental production rate determinations of Poreda and Cerling (1992) and Cerling and Craig (1994) in order to provide consistent ^3He and ^{21}Ne exposure ages. Scaling for altitude and latitude was performed according to Stone

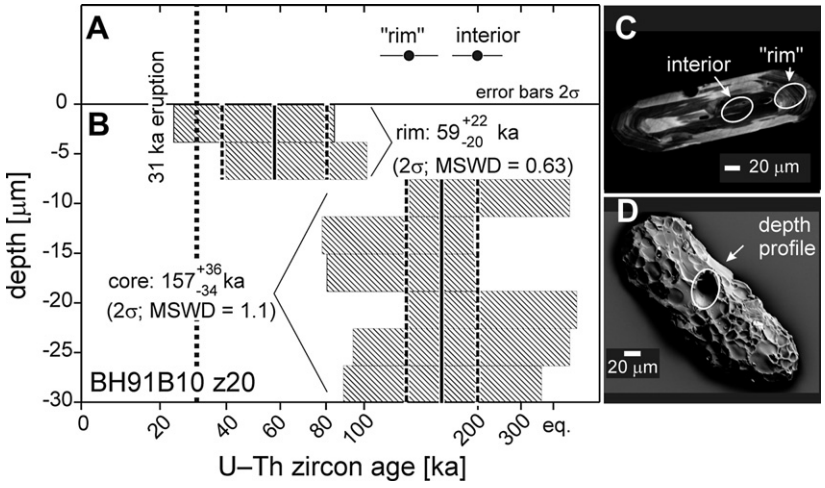

Fig. 4. U–Th zircon crystallization ages for grain BH91B10 z20 in spot analysis of crystal interiors (A), and depth profiling (B). Cathodoluminescence image of grain interior exposed by grinding and polishing (C), and original crystal surface in backscatter electron imaging (D). Locations of core and rim, as well as depth profiling analysis spots are indicated. Eruption age is indicated based on disequilibrium-corrected (U–Th)/He zircon ages.

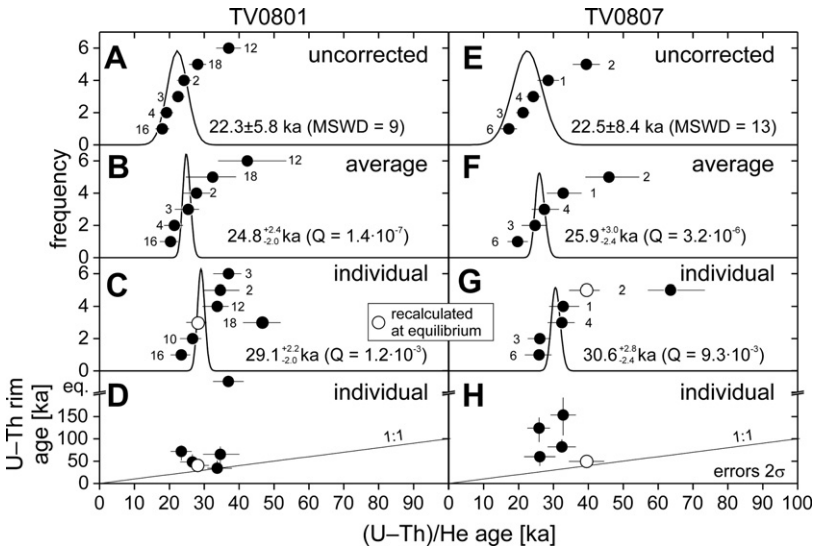

Fig. 5. (U–Th)/He ages and average age relative probability curves for TV0801 (A–D) and TV0807 (E–H). (U–Th)/He ages uncorrected for disequilibrium with weighted averages and values for mean square of weighted deviates (MSWD). Uncorrected data in (A and E) show high MSWD values, suggesting scatter due to disequilibrium in young zircon. Disequilibrium-corrected (U–Th)/He ages using an average crystallization age of 146 ± 110 ka from U–Th zircon analysis (B and F) still yield poor model fits ($Q < 0.001$) for both samples. Individually disequilibrium-corrected (U–Th)/He ages using U–Th rim ages (closed symbols) yield acceptable fits ($Q > 0.001$) when outliers TV0801 z18 and TV0807 z2 are adjusted assuming equilibrium (open symbols; C and G). This is supported by plotting U–Th zircon crystallization vs. individually disequilibrium-corrected (U–Th)/He eruption ages (D and H), where all zircon crystals satisfy the condition that eruption must post-date crystallization (i.e., the data plot above the 1:1 line). Otherwise, applying a disequilibrium correction based on the rim U–Th crystallization would result in overcorrection of crystals TV0801 z6 and TV0807 z2 whose interior may be much older (see also Fig. 4).

(2000); the corresponding scaling factors are also shown in Table 3. Corrections for horizon shielding are negligible, and self-shielding of the <5 cm samples was not accounted for as the cosmic-ray neutron flux is expected to be constant in the topmost few centimeters of rock (Masarik and Reedy, 1995). The resulting ^{3}He and ^{21}Ne exposure ages (Table 3) are between ~22 and 42 ka. The 2σ uncertainties are relatively large for ^{21}Ne (~15–90%); however the ^{3}He ages are quite precise, and the ^{3}He and ^{21}Ne ages are consistent for each sample. Systematic uncertainties of production rates and scaling factors are not included in the error limits of the exposure ages. For example, if ^{3}He production rates were higher than assumed here (e.g. Blard et al., 2006), the ages might decrease by ~10%. Likewise, accounting for geomagnetic field variations in the past 22–42 ka would increase production rates and therefore decrease exposure ages by ~2–6% (Masarik et al., 2001) at the latitude of Tres Vírgenes.

5. Discussion

5.1. Combined U–Th and (U–Th)/He zircon geochronology

New and published zircon results for La Virgen tephra indicate the presence of a complex zircon population that includes xenocrysts and Late Pleistocene crystals that pre-date the eruption by up to ~200 ka. Depth profiling demonstrates that protracted crystallization can be recorded in a single grain. This has implications for correcting (U–Th)/He ages for disequilibrium because interior crystallization ages are unknown, unless continuous age spectra for individual grains are obtained by depth profiling. This is, however, impractical because of long analysis durations (~10 μm/h sputter rate) that limit efficient sampling. U–Th rim analysis of zircon provides a minimum estimate for the age of the zircon, and allows screening for older grains that are closer to secular

Table 2
Results of He and Ne analyses in olivine/pyroxene separates from basaltic-andesitic surface rocks. Noble gas concentrations are in units of cm^3 STP/g, error limits are 2σ.

Sample Weight	T °C	^{4}He (10^{-8})	^{20}Ne (10^{-12})	^{3}He/^{4}He (10^{-6})	^{22}Ne/^{20}Ne (10^{-2})	^{21}Ne/^{20}Ne (10^{-2})
TV0802 0.98608 g	600	0.0350 ± 0.0019	112.2 ± 5.7	17.5 ± 7.0	10.18 ± 0.13	0.294 ± 0.014
	900	0.1495 ± 0.0075	90.7 ± 4.7	67.6 ± 6.7	10.23 ± 0.12	0.300 ± 0.014
	1750	1.450 ± 0.073	37.5 ± 2.1	12.00 ± 0.64	10.35 ± 0.19	0.426 ± 0.018
	Total	1.635 ± 0.073	240.4 ± 7.7	17.20 ± 0.91	10.23 ± 0.08	0.317 ± 0.009
1.07908 g	Crushed	0.639 ± 0.032	137.1 ± 7.1	10.4 ± 1.1	10.219 ± 0.069	0.2980 ± 0.0083
TV0808 1.49926 g	600	0.00673 ± 0.00051	24.0 ± 1.3	16 ± 13	10.20 ± 0.18	0.298 ± 0.019
	900	0.1040 ± 0.0052	210 ± 11	170 ± 12	10.078 ± 0.049	0.2941 ± 0.0063
	1750	0.235 ± 0.012	68.3 ± 3.5	25.6 ± 3.7	10.35 ± 0.10	0.375 ± 0.011
	Total	0.346 ± 0.013	302 ± 12	68.9 ± 4.9	10.149 ± 0.043	0.3127 ± 0.0053
1.00896 g	Crushed	0.229 ± 0.012	223 ± 12	9.5 ± 1.7	10.183 ± 0.048	0.294 ± 0.010
TV0811 0.65236 g	600	0.0753 ± 0.0042	129.3 ± 6.8	46.7 ± 9.7	10.18 ± 0.11	0.296 ± 0.015
	900	0.0528 ± 0.0030	64.6 ± 3.7	132 ± 13	10.26 ± 0.10	0.295 ± 0.018
	1750	0.0428 ± 0.0069	116.3 ± 6.2	27.6 ± 6.2	10.30 ± 0.11	0.322 ± 0.016
	Total	0.1709 ± 0.0086	310.2 ± 9.9	68.3 ± 6.4	10.242 ± 0.065	0.306 ± 0.009
0.65966 g	Crushed	0.0206 ± 0.0019	305 ± 16	4.8 ± 3.8	10.124 ± 0.090	0.296 ± 0.013

Sample locations (WGS-84 datum): TV0802 = N27°24′11″, W112°38′07″, 342 m elevation; TV0808 = N27°21′33″, W112°35′11″, 503 m elevation; TV0811 = N27°26′04″, W112°33′03″, 412 m elevation.

Table 3
Concentrations of cosmogenic ^{3}He and ^{21}Ne, adopted ^{3}He and ^{21}Ne production rate values (P_3 and P_{21}) for sea level and high latitude (as calculated from elemental composition according to Fenton et al., 2009), altitude/latitude scaling factors (Stone, 2000), and resulting ^{3}He and ^{21}Ne exposure ages (T_3 and T_{21}). Cosmogenic ^{3}He concentrations have been corrected for radiogenic ^{4}He (Blard and Farley, 2008) using R factors shown in Table 4. Asymmetric uncertainties for $^{21}Ne_c$ are caused by atmosphere-like ^{21}Ne/^{20}Ne ratios in the 600 °C and 900 °C steps (Table 2), for which only the fraction of the uncertainty range reaching above atmospheric was taken into account as lower-than-atmospheric ^{21}Ne/^{20}Ne is physically unreasonable.

Sample	$^{3}He_c$	$^{21}Ne_c$	P_3	P_{21}	Scaling factor	T_3	T_{21}
	10^6 atoms/g		at g^{-1} a^{-1}			ka	
TV0802	3.16 ± 0.54	$1.41^{+0.54}_{-0.21}$	119.5	44.7	1.037	25.5 ± 4.4	$30.4^{+11.6}_{-4.5}$
TV0808	5.75 ± 0.52	$1.46^{+0.35}_{-0.22}$	115.5	30.3	1.172	42.5 ± 3.8	$41.1^{+9.9}_{-6.2}$
TV0811	2.78 ± 0.32	$0.83^{+0.79}_{-0.51}$	115.7	27.5	1.095	22.0 ± 2.5	28^{+26}_{-17}

equilibrium, thus mitigating the effects of disequilibrium on (U–Th)/He ages.

Our new Monte Carlo computation of (U–Th)/He zircon eruption ages provides a rapid way of assessing the homogeneity of age populations. Data from La Virgen tephra show that (U–Th)/He eruption ages can be overcorrected if the rim age is used as representative for the entire grain, but replicate (U–Th)/He analyses of zircon with a range of rim crystallization ages (or preferentially magmatic xenocrysts in secular equilibrium) allow to identify such grains.

5.2. The age of La Virgen tephra

Based on the combined (U–Th)/He zircon results for proximal and distal La Virgen tephra (locations TV0801 and BH91B10), we recalculate the eruption age at $30.7^{+1.8}_{-1.4}$ ka ($n = 14$; $Q = 0.0014$). For this, we used data from Table 1 and those published in Schmitt et al. (2006). Because individual crystallization age constraints were in part lacking for our previous data, we used an average crystallization age (146 ± 110 ka) for the Schmitt et al. (2006) zircon crystals.

This age overlaps within uncertainty with the previously reported eruption age for La Virgen tephra (36 ± 6 ka; Schmitt et al., 2006). We also find no difference between the age of the TV0801 tephra at the ^{14}C charcoal site of Capra et al. (1998), and the proximal BH91B10 tephra previously analyzed (Schmitt et al., 2006), indicating that they represent the same eruption. Furthermore, both samples overlap in age with silicic tephra sample TV0807 from the vicinity of the Tres Tortugas domes where it underlies more mafic tephra. The extent of the overlying mafic tephra and its origin remains unconstrained. Based on its comparatively old surface exposure age ($T_3 = 42.5 \pm 3.8$ ka; TV0808), the southernmost dome can be ruled out as the source of the mafic tephra, leaving the middle or the northern dome as potential sources.

Our new data rule out the possibility that the sampling sites of Capra et al. (1998) and Schmitt et al. (2006) represent separate eruptions. The ambiguity arising from conflicting (U–Th)/He zircon and ^{14}C ages is further resolved by new surface exposure ages for mafic lavas (TV0802 and TV0811) that confirm a previous cosmogenic dating result (Hausback and Abrams, 1996). Both lavas lack tephra cover, and in the case of the Highway Basalt flow are entirely surrounded by La Virgen tephra. The younger exposure ages of both mafic lava flows ($T_3 = 25.5 \pm 4.4$ ka and 22.0 ± 2.5 ka) are stratigraphically consistent with the eruption age for La Virgen tephra, although these ages need to be considered as minimum ages for the emplacement if erosion had occurred. The much younger ^{14}C charcoal age for La Virgen tephra, however, violates the ^{3}He and ^{21}Ne age constraints for the overlying basalt flows.

(U–Th)/He zircon ages in sample TV0801 shed additional light on the problem of a conflictingly young ^{14}C charcoal age. Old (U–Th)/He zircon ages of ~1 Ma and ~22 Ma in TV0801 match ages of nearby exposed silicic tuffs from La Reforma caldera and Comondú volcanics, respectively (Sawlan, 1986; Schmitt et al., 2006). Such comparatively old (U–Th)/He zircon ages therefore are geologically reasonable, and they are reproducible. This argues against partial degassing of zircon during eruption or emplacement of the tephra, and is entirely consistent with a complete lack of reheating above the closure temperature for He in zircon (~180 °C; Reiners et al., 2004) at the time of the La Virgen eruption. We consequently interpret these grains as derived from fluvial reworking of sediment after the La Virgen eruption, and therefore of detrital origin. By contrast, proximally sampled tephra shows no evidence for zircon crystals with old (U–Th)/He ages (Schmitt et al., 2006), and all inherited crystals are completely reset with regard to (U–Th)/He. The presence of detrital zircon in TV0801 thus implies significant reworking of La Virgen tephra at the ^{14}C charcoal site. Field observations such as poor sorting of the deposit, mixing between sand and pumice, subtle rounding of pumice clasts, and deposition within an abandoned fluvial terrace strongly support this notion. This raises suspicion about the charcoal dated by Capra et al. (1998) of being detrital and unrelated to the eruption of La Virgen tephra. We thus reaffirm our conclusion in Schmitt et al. (2006) to disregard the ^{14}C charcoal date as an eruption age, and emphasize that the voluminous explosive eruption of La Virgen is pre-Holocene. Holocene summit eruptions as postulated by Sawlan (1986) presently remain an untested hypothesis.

Table 4
Concentrations of Th and U (ppm) in the mafic matrix and in the mineral separates of the investigated surface samples, as determined by ICP mass spectrometry. R factors (Blard and Farley, 2008) were calculated assuming a stopping distance of α particles of 20 μm and an average crystal diameter of 350 μm, and were assigned a conservative uncertainty of $(1 - R)/2$.

Sample	Matrix		Phenocrysts		R
	Th	U	Th	U	
TV0802	0.67	0.29	0.05	0.02	0.982 ± 0.009
TV0808	2.3	0.8	0.14	0.07	0.949 ± 0.026
TV0811	2.0	0.6	0.11	0.04	0.960 ± 0.020

Table 5
Concentrations of major elements and olivine and pyroxene mineral fractions (all in wt.%) in the investigated mineral separates, as determined by microprobe analysis and used for calculation of ^{3}He and ^{21}Ne production rates (Table 3) after Fenton et al. (2009).

Sample	O	Na	Mg	Al	Si	Ca	Ti	Fe	ol	px
TV0802	42.7	0.04	25.3	0.32	19.2	2.13	0.10	10.03	87	13
TV0808	42.7	0.17	14.5	0.88	22.4	10.83	0.25	8.02	30	70
TV0811	43.4	0.18	12.0	1.02	24.4	10.35	0.35	8.03	3	97

6. Conclusions

Combined U–Th and (U–Th)/He zircon geochronology using single crystal analysis provides concordant and internally consistent constraints for crystallization and eruption ages of Quaternary volcanic systems. Corrections of (U–Th)/He data for U-series disequilibrium are based on rim U–Th ages that are regarded as minimum crystallization ages. Zircon age zonations add uncertainty to disequilibrium corrections, but overcorrection can be identified by poor overlap between individual crystal ages. Because U-series disequilibrium is mitigated by long crystal residence, the recommended strategy is to select the oldest juvenile or xenocrystic zircon identified by U–Th rim analysis for (U–Th)/He

dating. Disequilibrium-corrected (U–Th)/He zircon dating yields reproducible ages that average $30.7^{+1.8}_{-1.4}$ ka ($n = 14$; $Q = 0.0014$), combining crystals from proximal and distal sampling locations. This age is stratigraphically consistent with ^{3}He and ^{21}Ne surface exposure ages of overlying mafic lava flows. Slightly older dome lavas occur south of Las Tres Vírgenes volcano. Undegassed zircon in La Virgen tephra from the location that yielded a ^{14}C-dated charcoal fragment (Capra et al., 1998) are strong indications for detrital contamination. We thus call for disregarding the previously published Holocene ^{14}C age for La Virgen tephra.

Acknowledgements

We thank Chris Farrar and Felix Wicke for assistance during field work, Tracy Howe for mineral separation, Roman Kislitsyn for (U–Th)/He analysis, Frank Kyte for electron probe analysis, Heike Rothe for ICP-MS measurements, and Enzio Schnabel for performing the noble gas analyses. Janet C. Harvey is acknowledged for generating the DEM plot. Pierre-Henri Blard is thanked for a helpful review. The ion microprobe facility at UCLA is partly supported by a grant from the Instrumentation and Facilities Program, Division of Earth Sciences, National Science Foundation.

Editorial handling by: D. Bourlès

References

Bateman, H., 1910. The solution of a system of differential equations occurring in the theory of radio-active transformations. Proceedings of the Cambridge Philosophical Society 15, 423–427.

Biswas, S., Coutand, I., Grujic, D., Hager, C., Stockli, D., Grasemann, B., 2007. Exhumation and uplift of the Shillong plateau and its influence on the eastern Himalayas: new constraints from apatite and zircon (U–Th–[Sm])/He and apatite fission track analyses. Tectonics 26 (6), TC6013. doi:10.1029/2007TC002125.

Blard, P.-H., Farley, K.A., 2008. The influence of radiogenic ^{4}He on cosmogenic ^{3}He determinations in volcanic olivine and pyroxene. Earth and Planetary Science Letters 276 (1–2), 20–29.

Blard, P.-H., Pik, R., Lavé, J., Bourlès, D., Burnard, P.G., Yokochi, R., Marty, B., Trusdell, F., 2006. Cosmogenic ^{3}He production rates revisited from evidences of grain size dependent release of matrix-sited helium. Earth and Planetary Science Letters 247, 222–234.

Capra, L., Macias, J.L., Espindola, J.M., Siebe, C., 1998. Holocene plinian eruption of La Virgen volcano, Baja California, Mexico. Journal of Volcanology and Geothermal Research 80 (3–4), 239–266.

Capra, L., Siebe, C., Macias, J.L., Espindola, J.M., 2007. Comment on: Schmitt, AK et al. (2006): Eruption and magma crystallization ages of Las Tres Vírgenes (Baja California) constrained by combined ^{230}Th/^{238}U and (U–Th)/He dating of zircon [J. Volcanol. Geotherm. Res. 158: 281–295]. Journal of Volcanology and Geothermal Research 163 (1–4), 98–101.

Cerling, T.E., Craig, H., 1994. Cosmogenic ^{3}He production rates from 39°N to 46°N latitude, western USA and France. Geochimica et Cosmochimica Acta 58 (1), 249–255.

Demant, A., 1981. Plio-Quaternary volcanism of the Santa Rosalia area, Baja California, Mexico. In: Ortlieb, L., Roldan-Quintana, J. (Eds.), Geology of Northwestern Mexico and Southern Arizona, Field Guides and Papers. U.N.A.M, Inst. Geol., Estación Regional del Noroeste, Mexico City, Mexico D.F., pp. 295–307.

Fabriol, H., Delgado-Argote, L.A., Danobeitia, J.J., Cordoba, D., Gonzalez, A., Garcia-Abdeslem, J., Bartolome, R., Martin-Atienza, B., Frias-Camacho, V., 1999. Backscattering and geophysical features of volcanic ridges offshore Santa Rosalia, Baja California Sur, Gulf of California, Mexico. Journal of Volcanology and Geothermal Research 93 (1–2), 75–92.

Farley, K.A., Wolf, R.A., Silver, L.T., 1996. The effects of long alpha-stopping distances on (U–Th)/He ages. Geochimica et Cosmochimica Acta 60 (21), 4223–4229.

Farley, K.A., Kohn, B.P., Pillans, B., 2002. The effects of secular disequilibrium on (U–Th)/He systematics and dating of Quaternary volcanic zircon and apatite. Earth and Planetary Science Letters 201 (1), 117–125.

Fenton, C.R., Niedermann, S., Goethals, M., Schneider, B., Wijbrans, J., 2009. Evaluation of cosmogenic ^{3}He and ^{21}Ne production rates in olivine and pyroxene from two Pleistocene basalt flows, western Grand Canyon, AZ, USA. Quaternary Geochronology 4, 475–492.

Garduno-Monroy, V.H., Vargas-Ledezma, H., Campos-Enriquez, J.O., 1993. Preliminary geologic studies of Sierra El Aguajito (Baja California, Mexico): a resurgent-type caldera. Journal of Volcanology and Geothermal Research 59 (1–2), 47–58.

Hausback, B.P., Abrams, M.J., 1996. Plinian eruption of La Virgen Tephra, Volcan Las Tres Vírgenes, Baja California Sur, Mexico. Eos, Transactions, American Geophysical Union 77 (46 Suppl.), 813–814.

Ives, R.L., 1962. Dating of the 1746 eruption of Tres Vírgenes volcano, Baja California del Sur, Mexico. Geological Society of America Bulletin 73 (5), 647–648.

Kober, F., Ivy-Ochs, S., Leya, I., Baur, H., Magna, T., Wieler, R., Kubik, P.W., 2005. In situ cosmogenic ^{10}Be and ^{21}Ne in sanidine and in situ cosmogenic ^{3}He in Fe–Ti-oxide minerals. Earth and Planetary Science Letters 236 (1–2), 404–418.

Krogh, T.E., 1973. Low-contamination method for hydrothermal decomposition of zircon and extraction of U and Pb for isotopic age determinations. Geochimica et Cosmochimica Acta 37 (3), 485–494.

Licciardi, J.M., Kurz, M.D., Clark, P.U., Brook, E.J., 1999. Calibration of cosmogenic ^{3}He production rates from Holocene lava flows in Oregon, USA, and effects of the Earth's magnetic field. Earth and Planetary Science Letters 172 (3–4), 261–271.

Masarik, J., 2002. Numerical simulation of in-situ production of cosmogenic nuclides. Geochimica et Cosmochimica Acta 66 (15A), A491.

Masarik, J., Reedy, R.C., 1995. Terrestrial cosmogenic-nuclide production systematics calculated from numerical simulations. Earth and Planetary Science Letters 136 (3–4), 381–395.

Masarik, J., Frank, M., Schäfer, J.M., Wieler, R., 2001. Correction of in situ cosmogenic nuclide production rates for geomagnetic field intensity variations during the past 800,000 years. Geochimica et Cosmochimica Acta 65, 2995–3003.

Niedermann, S., Bach, W., Erzinger, J., 1997. Noble gas evidence for a lower mantle component in MORBs from the southern East Pacific Rise: decoupling of helium and neon isotope systematics. Geochimica et Cosmochimica Acta 61 (13), 2697–2715.

Niedermann, S., Schaefer, J.M., Wieler, R., Naumann, R., 2007. The production rate of cosmogenic ^{38}Ar from calcium in terrestrial pyroxene. Earth and Planetary Science Letters 257 (3–4), 596–608.

Paces, J.B., Miller Jr., J.D., 1993. Precise U–Pb ages of Duluth Complex and related mafic intrusions, northeastern Minnesota; geochronological insights to physical, petrogenetic, paleomagnetic, and tectonomagnetic processes associated with the 1.1 Ga Midcontinent Rift System. Journal of Geophysical Research, B, Solid Earth and Planets 98 (8), 13997–14013.

Poreda, R.J., Cerling, T.E., 1992. Cosmogenic neon in recent lavas from the western United States. Geophysical Research Letters 19 (18), 1863–1866.

Press, W.H., Teukolsky, S.A., Vetterling, W.T., Flannery, B.P., 2002. Numerical Recipes: The Art of Scientific Computing. Cambridge University Press, New York.

Reiners, P.W., Spell, T.L., Nicolescu, S., Zanetti, K.A., 2004. Zircon (U–Th)/He thermochronometry: He diffusion and comparisons with ^{40}Ar/^{39}Ar dating. Geochimica et Cosmochimica Acta 68 (8), 1857–1887.

Sawlan, M.G., 1986. Petrogenesis of Late Cenozoic volcanic rocks from Baja California Sur, Mexico. Doctoral, University of California.

Schäfer, J.M., Ivy-Ochs, S., Wieler, R., Leya, J., Baur, H., Denton, G.H., Schlüchter, C., 1999. Cosmogenic noble gas studies in the oldest landscape on earth: surface exposure ages of the Dry Valleys, Antarctica. Earth and Planetary Science Letters 167 (3–4), 215–226.

Schmitt, A.K., Stockli, D.F., Hausback, B.P., 2006. Eruption and magma crystallization ages of Las Tres Vírgenes (Baja California) constrained by combined ^{230}Th/^{238}U and (U–Th)/He dating of zircon. Journal of Volcanology and Geothermal Research 158 (3–4), 281–295.

Schmitt, A.K., Stockli, D.F., Hausback, B.P., 2007. Reply to comment by: Lucia Capra, Claus Siebe, Jose Luis Macias, and Juan Manuel Espindola. Journal of Volcanology and Geothermal Research 163 (1–4), 102–103.

Stone, J.O., 2000. Air pressure and cosmogenic isotope production. Journal of Geophysical Research, B, Solid Earth and Planets 105 (B10), 23753–23759.

Verma, S.P., Pandarinath, K., Santoyo, E., Gonzalez-Partida, E., Torres-Alvarado, I.S., Tello-Hinojosa, E., 2006. Fluid chemistry and temperatures prior to exploitation at the Las Tres Vírgenes geothermal field, Mexico. Geothermics 35 (2), 156–180.

Wiedenbeck, M., Hanchar, J.M., Peck, W.H., Sylvester, P., Valley, J., Whitehouse, M., Kronz, A., Morishita, Y., Nasdala, L., Fiebig, J., Franchi, I., Girard, J.P., Greenwood, R.C., Hinton, R., Kita, N., Mason, P.R.D., Norman, M., Ogasawara, M., Piccoli, P.M., Rhede, D., Satoh, H., Schulz-Dobrick, B., Skar, O., Spicuzza, M.J., Terada, K., Tindle, A., Togashi, S., Vennemann, T., Xie, Q., Zheng, Y.F., 2004. Further characterisation of the 91500 zircon crystal. Geostandards and Geoanalytical Research 28 (1), 9–39.